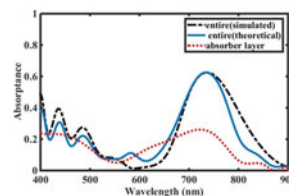# Angular and Wavelength Simultaneous Selection in Transparent OPVs Based on Near-Infrared Bragg Reflector and Antireflection Coating

Zhongchao Wei
Yuebo Liu
Shuyuan Xiao
Xianping Li
Nianfa Zhong
Hongzhan Liu
Faqiang Wang
Ruisheng Liang
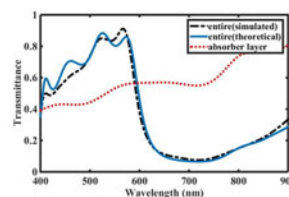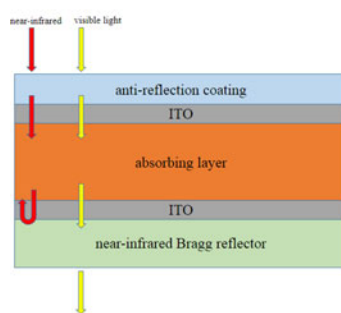
Angular and Wavelength Simultaneous Selection in Transparent OPVs Based on Near-Infrared Bragg Reflector and Antireflection Coating

Zhongchao Wei,[1] **Yuebo Liu,**[1] **Shuyuan Xiao,**[2] **Xianping Li,**[1]
Nianfa Zhong,[1] **Hongzhan Liu,**[1] **Faqiang Wang,**[1]
and Ruisheng Liang[1]

[1]Guangdong Provincial Key Laboratory of Nanophotonic Functional Materials and Devices,
School for Information and Optoelectronic Science and Engineering, South China Normal
University, Guangzhou 510006, China
[2]Wuhan National Laboratory for Optoelectronics, Huazhong University of Science and
Technology, Wuhan 430074, China

Abstract: A novel design based on genetic algorithm is proposed to construct a near-infrared Bragg reflector and an antireflection coating, which are supposed to be applied in the transparent organic photovoltaics. By incorporating the absorbing layer which composed of ClAlPc/C_{60} with the structure designed, it leads to a significant near-infrared absorption increase from 16.6% to 36.3% within 650–850 nm and high average visible-transparency of 72% within 400–580 nm at normal incidence. Moreover, the near-infrared absorption increases with the enlargement of the incident angle from 0° to 30°, where the average transmittance remains above 60% simultaneously. This design can further improve the balance between transparency in the visible for scenic sight view and sunlight absorption in near-infrared for high-efficiency electricity generation. The potential of adopting this novel design on transparent building-integrated photovoltaic modules, which dominate the landscape of the major cities, is tremendous.

Index Terms: Genetic algorithm, Bragg reflector, Simultaneous selection, Transparent Organic photovoltaic.

1. Introduction

Over the past three decades, the organic photovoltaic field has been widely applied in electricity generation configurations where silicon technology is not suitable [1], [2]. For instance, to integrate photovoltaic panels onto window panes in buildings, skyscrapers, and automobiles, enhancing the functionality of already utilized transparent surfaces, organic photovoltaic is necessary [3]. When thin film solar cell performance is evaluated in terms of the device's visible transparency and power conversion efficiency, transparent organic photovoltaics (OPVs) offer the most promising solution [4].
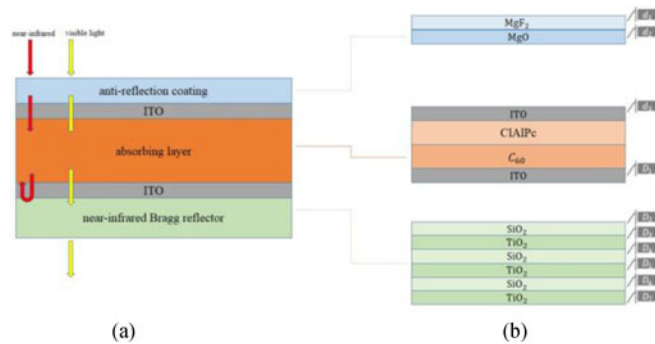
Fig. 1. (a) Schematic diagram of a three-tier structure. (b) Detailed view of the entire structure.

In prior studies, three categories of approaches have been consolidated in the fabrication of high performance OPVs [5]: The first is to reduce the band gap of the absorbing layer of OPVs to obtain lower absorption in the visible region [6]–[10], such as chloroaluminium phthalocyanine (ClAlPc) [11], Its band gap has been successfully pushed from the near ultraviolet or visible toward the near-infrared region. Lunt and Bulovic [13] demonstrated the use of chloroaluminum phthalocyanine (ClAlPc) as donor in a planar double heterojunction OPV and employing C_{60} as acceptor, which shows the absorption peaks in 650–850 nm, meanwhile permitted high transmission in the visible region, making objects can be seen clearly and appeared unaltered in shape or color to viewers. The second approach is to incorporate with anti-reflection coatings for decreasing surface reflectance of OPVs in the visible region or in Bragg reflectors to trap the near ultraviolet and near-infrared light in the near-infrared region [12]–[19]. The last is to enclose the active layer in a Fabry–Perot type cavity formed by two metallic semi-transparent electrodes to get high power conversion efficiency [20], [21].

In this paper, the first and second approach is combined to improve the performance of the near-infrared absorbing transparent OPVs. Incorporating the OPVs' absorbing layer which composed of $ClAlPc/C_{60}$ with an anti-reflection coating and a near-infrared Bragg reflector, we can further improve the balance between transparency in the visible and absorption in near-infrared. Here, genetic algorithm [22] is used to design the structures, and the ad hoc nonperiodic structures are found in the end. An inverse integration design is used to determine each layer's thickness specifically to get the optimal performance. The entire structure can simultaneously enhance the transmission in the visible region as well as the absorption in the near-infrared region. Contrasted with the results of ref [13], the average visible transmittance can be increased by 31% and has very little impact on absorption in near-infrared. Contrasted with the result of [12]. This design is more targeted to improve the overall performance in the visible and near-infrared region.

2. Structure

The design model is a three-tier structure, as shown in Fig. 1(a). The first tier is an anti-reflection coating. The absorbing layer and the transparent conductive oxide (TCO) layers are situated in the second tier. The third tier is a near-infrared Bragg reflector. The sunshine comes through the surface of the anti-reflection coating, which will enhance the transmission in the visible and near-infrared region. The near-infrared Bragg reflector can reflect only the near-infrared light back to enhance the near-infrared absorption with a high average simultaneous visible-transparency.

In order to reduce the loss of light energy, dielectric materials with near-zero extinction coefficient are adopted in the novel design. The detailed structure is shown in Fig. 1(b). The anti-reflection coating is composed of the first layer of MgF2 and the second layer of MgO. The thicknesses of each layer are expressed as d1 and d2, respectively. The layer between the anti-reflection coating and the absorbing layer is a TCO layer, which is made with indium tin oxides (ITO). The thickness
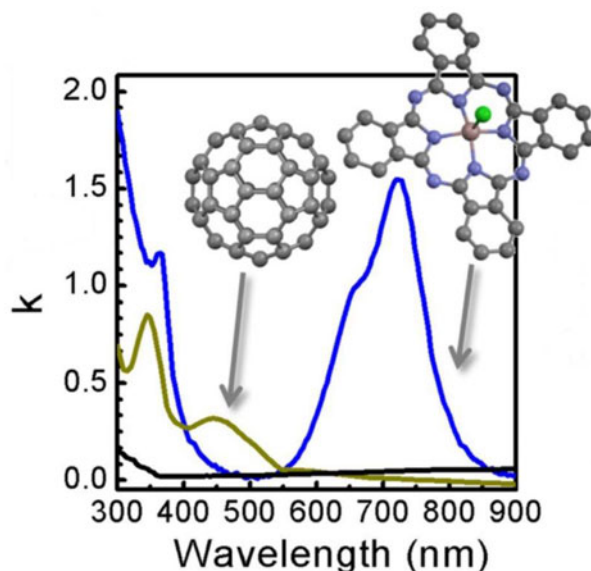
Fig. 2. K means the imaginary part of complex index of refraction; for the absorbing layer, the ClAlPc (blue line) is donor, C_{60} (olive line) is acceptor, and sputtered ITO (black line).

of the ITO film is expressed as d3. Another TCO layer lies between the absorbing layer and the near-infrared Bragg reflector. It's also made with ITO and the thickness expressed as D1. In creating a Bragg reflector which reflects strongly in the near-infrared region, the materials are chosen to be SiO2 and TiO2, which are both readily available common materials for making a reflector within the target wavelength range. The Bragg reflector consists of three bilayers, the thicknesses of each layer are expressed as D2, D3 . . . D7, respectively.

The absorbing layer is ClAlPc(15 nm)/C60(30 nm), the photoelectrical parameters of the absorbing layer is obtained from Fig. 2. as Richard R. Lunt *et al*. reported [13].

3. Theoretical Analysis

In this work, genetic algorithm (GA) is used to design the structure. GA is essentially mimicking the process of natural evolution, in which the fitness of an individual is improved by successive iteration through the processes of selection, crossover and mutation. The implementation of GA for the design structure requires an appropriate selection of various parameters. Air is considered as the ambient medium. The thickness of each layer is considered as a variable parameter and optimized by continuous evolution. The range of the minimum and maximum thicknesses of dielectric materials in layers is the search space of the variable parameter. The maximum thickness of the layer is set to 450 nm and the minimum thickness is set to 20 nm. Besides, the number of layers and sequence is assumed to be fixed as showed in Fig. 1. The other parameters such as the mutation rate, crossover rate, migration rate and population size are also fixed and types of them are the default throughout the optimization process. The values of mutation rate, crossover rate, migration rate per 20 generations, and population size are set to 1%, 80%, 20%, and 200, respectively. At the beginning of the optimization process, an initial population with a fixed number of layers within the range of layer thicknesses [20 nm, 450 nm] is generated. After the generation of the initial population, each individual is evaluated, individuals of excellent performance are subjected to the selection, crossover and mutation operators to reproduce a new population of the next generation. Then the iterative process can be continued until the optimal individual is met. The evaluation of the performance of each individual is performed by a suitable figure of merit function, also called the 'fitness function.' The optimal individual will be obtained when the value of fitness function has little change as the increase of iteration time.

The optical properties of each layer r $(r = 1, 2, \ldots, m)$ are described by its complex index of refraction $\tilde{n}_r = n_r + jk_r$, which is a function of the wavelength of the incident light. The optical properties of dielectric materials and TCO layers can be obtained in the refractive-index-database of filmetrics [23]. The optical properties of the absorbing layer can be got from [11] and [13].

The layer phase thickness is defined by

$$\delta_r = \frac{2\pi}{\lambda} n_r d_r \cos \theta_r \tag{1}$$

which corresponds to the phase change as the wave traverses layer, here θ_r is the angle of refraction in layer r.

For p-polarized, the admittance is expressed as

$$\eta_r = \frac{n - jk}{\cos \delta_r} \tag{2a}$$

and for s-polarized, it is expressed as

$$\eta_r = (n - jk) \cos \delta_r. \tag{2b}$$

By using the interface matrix and the layer matrix, the total system transfer matrix can be written as [24]

$$\begin{bmatrix} B \\ C \end{bmatrix} = \prod_{r=1}^{m} \begin{bmatrix} \cos \delta_r & \dfrac{j \sin \delta_r}{\eta_r} \\ j\eta_r \sin \delta_r & \cos \delta_r \end{bmatrix} \begin{bmatrix} 1 \\ \eta_{m+1} \end{bmatrix}. \tag{3}$$

For the total layered structure, the resulting complex reflectance R and transmittance T can be expressed by using the matrix elements of the total system transfer matrix of (3) as

$$R = \left(\frac{\eta_0 B - C}{\eta_0 B + C} \right) \left(\frac{\eta_0 B - C}{\eta_0 B + C} \right)^* \tag{4a}$$

$$T = \frac{4\eta_0 \eta_{m+1}}{(\eta_0 B + C)(\eta_0 B + C)^*}. \tag{4b}$$

In addition, η_0 is the admittance of the transparent ambient; then, the absorptance A can be expressed as

$$A = 1\text{-}R\text{-}T. \tag{4c}$$

Here, the anti-reflection coating and the first ITO film are taken as a whole; the fitness function can be defined as

$$F_1 = -\left(\frac{\sum_{\lambda=400}^{900} \sum_{10 \times \theta=0}^{10} T_s(\lambda_\theta, d) + \sum_{\lambda=400}^{900} \sum_{10 \times \theta=0}^{10} T_p(\lambda_\theta, d)}{501 \times 11 \times 2} \right)^2. \tag{5}$$

Here, $T_s(\lambda_\theta, d)$ is the value of s-polarized transmittance at wavelength λ (nm) and incident angle θ (rad) for a given set of layer thicknesses ($d = (d1, d2, d3)$) using the transfer matrix method, similarly the $T_p(\lambda_\theta, d)$ is the value of p-polarized.

The anti-reflection coating, in principle, the maximum transmittance is commended over the entire wavelength range and incident angle range of interest. Optimum structures design with maximum transmittance will have the minimum value of fitness function F_1. The minimum value can be obtained by the GA operation, with the evolution of populations, in the 70th population, and the value is found; then, the optimum individual $d = (d1, d2, d3)$ is given as

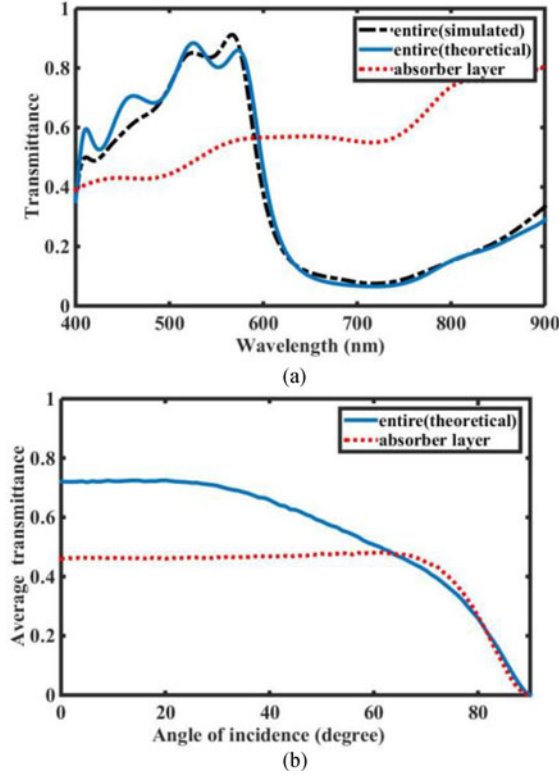$$d = (128.142 \text{ nm}, 77.074 \text{ nm}, 20 \text{ nm}).$$

Fig. 3. (a) Transmittance of an absorbing layer and the entire structure at normal incidence. (b) Average transmittance of an absorbing layer and the entire structure changed with angle of incidence in the 400–580 nm wavelength range.

Similarly, the second ITO film and the near-infrared Bragg reflector are taken as a whole, the fitness function is defined as

$$F_2 = -\left[\left(\frac{\sum_{\lambda=400}^{580}\left(T_s(\lambda, d) + T_p(\lambda, d)\right)}{181 \times 2}\right)^2 + \left(\frac{\sum_{\lambda=630}^{900}\sum_{10(\theta-0.5)=0}^{5}\left(R_s(\lambda_\theta, d) + R_p(\lambda_\theta, d)\right)}{271 \times 6 \times 2}\right)^2\right].$$
(6)

The $T_s(\lambda, D)$ is the calculated value of s-polarized transmittance at wavelength λ(nm) for a given set of layer thicknesses (D = (D1, D2…D7)) in normal incidence, and the $T_p(\lambda, D)$ is the value of p-polarized transmittance at the same condition. The $R_s(\lambda_\theta, D)$ is the value of s-polarized reflectance at wavelength λ(nm) and incident angle θ(rad) for a given set of layer thicknesses (D = (D1, D2…D7)), and $R_p(\lambda_\theta, D)$ is the value of p-polarized. The weights of two terms are equal; it can improve the balance between transmission in the visible region and absorption in the near-infrared region. The design can reflect the near-infrared light within 650–850 nm back into absorbing layer, while maintaining high visible-transparency within the 400-580 nm range. The optimum structure for the near-infrared Bragg reflector will have the minimum value of fitness function F_2, and the optimum individual D = (D1, D2…D7) is found in the 123th population by GA operation.

D = (20 nm, 311.598 nm, 79.488 nm, 124.265 nm, 73.268 nm, 122.684 nm, 81.981 nm).

4. Results and Discussions and Simulation

To confirm the performance of the design, a detailed analysis of the optical properties of the entire structure was made by using Lumerical FDTD Solutions and MATLAB, respectively. Therefore, we
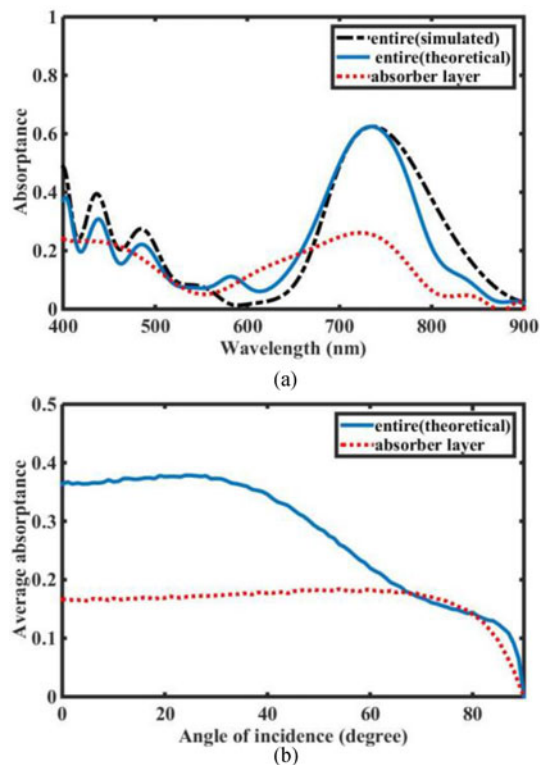
Fig. 4. (a) Absorptance of the single absorbing layer and entire structure at normal incidence. (b) Average absorptance of the single absorbing layer and entire structure changed with angle of incidence in 650–850 nm.

got the theoretical values of the optical properties by MATLAB, and simulated values by Lumerical FDTD Solutions. In Fig. 3(a), the dot dash black line and thin solid blue line represent the simulated values and the theoretical values of transmittance of the entire structure at normal incidence, respectively. The red dotted line represents the values of transmittance of the single absorbing layer at normal incidence. Comparing the transmittance of absorbing layer with that of the entire structure at normal incidence, the latter has significantly higher transmittance than the former in the wavelength range of 400–580 nm. Visible light in the entire structure is transmitted with 72% average intensity at normal incidence, whereas single absorbing layer is 45.9% in the same case, it means 1.57 times in improving the average transmittance of an absorbing layer. Contrasted with the result of ref [13], the value of average visible transmittance has been increased by 31% in the same condition.

The average transmittance of the absorbing layer and entire structure changes with the variations of the angle, within 400–580 nm range, is shown in Fig. 3(b). The value of average transmittance is obtained by Monte Carlo method [25]. With the enlargement of incidence angles, the trend line of the average transmittance of absorbing layer is low and even whereas the trend line of the average transmittance of entire structure decreases slowly and monotonously, but remain above 60% until the incident angle increases to 50°. These features make it possible to see objects clearly through the OPVs.

In Fig. 4(a), the dot dash black line and the thin solid blue line represent the simulated and theoretical absorption values of the entire structure at normal incidence, respectively. The red dotted line represents the value of absorptance of the single absorbing layer at normal incidence. Comparing the absorptance of absorbing layer with that of the entire structure at normal incidence, the latter has a much higher absorption than the former in the wavelength range of 650–850 nm. As showed in Fig. 4(b), the structures designed can make the average absorptance increases from
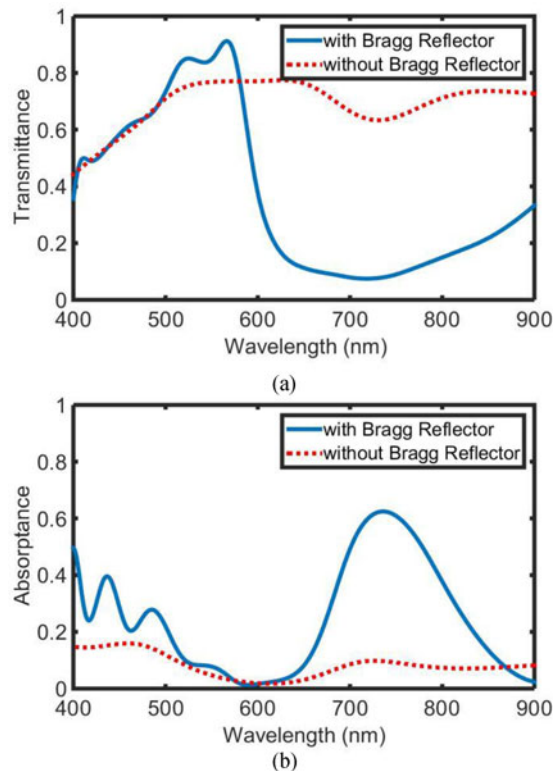
Fig. 5. (a) Transmittance of the device with and without Bragg reflector at normal incidence. (b) Absorptance of the device with and without Bragg reflector at normal incidence.

16.6% to 36.3% at normal incidence. Meanwhile, with the enlargement of the incidence angle, the average absorptance of the entire structure increases in the incident angle range of 0°–30°, then decreases slowly, but remains above 30% until the incident angle increases to 50°. These properties are very suitable for sunlight absorption.

In Fig. 5, the solid blue line represents the device with Bragg reflector and the red dotted line represents the device without Bragg Reflector. From Fig. 5(a) and (b), we can see that the Bragg reflector raise the transmittance of entire structure slightly in the wavelength range of 500–600 nm but, in the meantime, enhance the absorption significantly in the wavelength range of 650–850 nm. These two spectra indicated that the Bragg reflector play a very important role in near-infrared absorption.

5. Conclusion

In summary, we have demonstrated that the performance of OPVs can be improved significantly by incorporating the absorbing layer of OPVs with the anti-reflection coating and the near-infrared Bragg reflector, which makes the average absorptance of entire structure within 650–850 nm increases from 16.6% to 36.3% at normal incidence, with a simultaneous high average visible-transparency of 72% within 400–580 nm region. Meanwhile, average absorptance increases with the enlargement of the incidence angle in the incidence angle range of 0°–30°, after that decreases slowly, but remains above 30% until the incidence angle increases to 50°. The average transmittance will remain above 60% at the same time. These features are very helpful for the sunlight absorption and make it possible to clearly see objects through the OPVs. Besides, structures designed have little light absorption loss, since it consists of the dielectric materials with near-zero extinction coefficient. This design idea could also be applied to other special needs of the film system. It will provide good economic benefits and a wide scope of application.

Refererences

[1] J. Benemann, O. Chehab, and E. Schaar-Gabriel, "Building-integrated PV modules," *Solar Energy Mater. Solar Cells*, vol. 67, pp. 345–354, 2001.

[2] J. Hirvonen, G. Kayo, A. Hasan, and K. Sirén, "Zero energy level and economic potential of small-scale building-integrated PV with different heating systems in Nordic conditions," *Appl. Energy*, vol. 167, pp. 255–269, 2016.

[3] C. Tuchinda, S. Srivannaboon, and H. W. Lim, "Photoprotection by window glass, automobile glass, and sunglasses," *J. Amer. Acad. Dermatology*, vol. 54, pp. 845–854, 2006.

[4] J. Peng, D. C. Curcija, L. Lu, S. E. Selkowitz, H. Yang, and W. Zhang, "Numerical investigation of the energy saving potential of a semi-transparent photovoltaic double-skin facade in a cool-summer Mediterranean climate," *Appl. Energy*, vol. 165, pp. 345–356, 2016.

[5] P. Romero-Gómez *et al.*, "Semi-transparent polymer solar cells," *J. Photon. Energy*, vol. 5, 2015, Art. no. 057212.

[6] T. Tanaka *et al.*, "Enhanced red-light emission by local plasmon coupling of Au nanorods in an organic light-emitting diode," *Appl. Phys. Exp.*, vol. 4, 2011, Art. no. 032105.

[7] L. Dou, W. H. Chang, J. Gao, C. C. Chen, J. You, and Y. Yang, "A selenium-substituted low-bandgap polymer with versatile photovoltaic applications," *Adv. Mater.*, vol. 25, pp. 825–831, 2013.

[8] C.-C. Chen *et al.*, "Visibly transparent polymer solar cells produced by solution processing," *ACS Nano*, vol. 6, pp. 7185–7190, 2012.

[9] C. C. Chueh *et al.*, "Toward high-performance semi-transparent polymer solar cells: Optimization of ultra-thin light absorbing layer and transparent cathode architecture," *Adv. Energy Mater.*, vol. 3, pp. 417–423, 2013.

[10] Y. Shinmura, T. Yoshioka, T. Kaji, and M. Hiramoto, "Mapping of band-bending for doped C60 films," *Appl. Phys. Exp.*, vol. 7, 2014, Art. no. 071601.

[11] M. Azim-Araghi and A. Krier, "Optical characterization of chloroaluminium phthalocyanine (ClAlPc) thin films," *Pure Appl. Opt., J. Eur. Opt. Soc. Part A*, vol. 6, pp. 443–453, 1997.

[12] B. Roberts, D. Nanditha, M. Dissanayake, and P.-C. Ku, "Angular selective semi-transparent photovoltaics," *Opt. Exp.*, vol. 20, pp. A265–A269, 2012.

[13] R. R. Lunt and V. Bulovic, "Transparent, near-infrared organic photovoltaic solar cells for window and energy-scavenging applications," *Appl. Phys. Lett.*, vol. 98, 2011, Art. no. 113305.

[14] R. Betancur, P. Romero-Gomez, A. Martinez-Otero, X. Elias, M. Maymó, and J. Martorell, "Transparent polymer solar cells employing a layered light-trapping architecture," *Nature Photon.*, vol. 7, pp. 995–1000, 2013.

[15] P. Bermel, C. Luo, L. Zeng, L. C. Kimerling, and J. D. Joannopoulos, "Improving thin-film crystalline silicon solar cell efficiencies with photonic crystals," *Opt. Exp.*, vol. 15, pp. 16986–17000, 2007.

[16] W. Yu *et al.*, "Simultaneous improvement in efficiency and transmittance of low bandgap semitransparent polymer solar cells with one-dimensional photonic crystals," *Solar Energy Mater. Solar Cells*, vol. 117, pp. 198–202, 2013.

[17] W. Yu *et al.*, "Semitransparent polymer solar cells with one-dimensional (WO3/LiF) N photonic crystals," *Appl. Phys. Lett.*, vol. 101, 2012, Art. no. 153307.

[18] D.-D. Zhang *et al.*, "Enhanced performance of semitransparent inverted organic photovoltaic devices via a high reflector structure," *ACS Appl. Mater. Interfaces*, vol. 5, pp. 10185–10190, 2013.

[19] M. Yoshimura, E. Nakai, K. Tomioka, and T. Fukui, "Indium phosphide core–shell nanowire array solar cells with lattice-mismatched window layer," *Appl. Phys. Exp.*, vol. 6, 2013, Art. no. 052301.

[20] L. Zuo *et al.*, "Microcavity-enhanced light-trapping for highly efficient organic parallel tandem solar cells," *Adv. Mater.*, vol. 26, pp. 6778–6784, 2014.

[21] F. Pastorelli *et al.*, "Enhanced light harvesting in semitransparent organic solar cells using an optical metal cavity configuration," *Adv. Energy Mater.*, vol. 5, pp. 1400614(1–5), 2015.

[22] S. J. Patel and V. Kheraj, "Optimization of the genetic operators and algorithm parameters for the design of a multilayer anti-reflection coating using the genetic algorithm," *Opt. Laser Technol.*, vol. 70, pp. 94–99, 2015.

[23] [Online]. Available: http://www.filmetrics.com/refractive-index-database, 2015-08-16/2016-05-24.

[24] L. A. Pettersson, L. S. Roman, and O. Inganäs, "Modeling photocurrent action spectra of photovoltaic devices based on organic thin films," *J. Appl. Phys.*, vol. 86, pp. 487–496, 1999.

[25] N. Metropolis and S. Ulam, "The Monte Carlo method," *J. Amer. Statist. Assoc.*, vol. 44, pp. 335–341, 1949.